Optimization of Axial Pump Characteristic Dimensions and Induced Hemolysis for Mechanical Circulatory Support Devices

Theodosios Korakianitis,* Mohammad A. Rezaienia,† Gordon M. Paul,† Eldad J. Avital,† Martin T. Rothman,‡ and Sahand Mozafari†

The application of axial pumps as ventricular assist devices (VADs) requires significant modifications to the size and characteristics of industrial pumps due to the difference in flow fields of industrial and medical pumps. Industrial pumps operate in the region of Reynolds number Re = 108, whereas axial blood pumps operate in Re < 10^6. The common pump design technique is to rely on the performance of previously designed pumps using the concept of fluid dynamic similarity. Such data are available for industrial pumps as specific speed-specific diameter (n_s–d_s) graphs. The difference between the flow fields of industrial and medical pumps makes the industrial n_s–d_s graphs unsuitable for medical pumps and consequently several clinically available axial blood pumps operate with low efficiencies. In this article, numerical and experimental techniques were used to design 62 axial pump impellers with different design characteristics suitable for VADs and mechanical circulatory support devices (MCSDs). The impellers were manufactured and experimentally tested in various operating conditions of flow, pressure, and rotational speed. The hemocompatibility of the impellers was numerically investigated by modeling shear stress and hemolysis. The highest efficiency of each pump impeller was plotted on an n_s–d_s diagram. The nondimensional results presented in this article enable preliminary design of efficient and hemocompatible axial flow pumps for VADs and MCSDs. *ASAIO Journal* 2017; XX:00–00.

Key Words: ventricular assist device, mechanical circulatory support device, axial blood pump, hemolysis, specific speed, specific diameter

From the *Parks College of Engineering, Aviation and Technology, Saint Louis University, St. Louis, Missouri; †School of Engineering and Materials Science, Queen Mary University of London, London E1 4NS, United Kingdom; and ‡Department of Cardiology, Barts and the London NHS Trust, London Chest Hospital, London E2 9JX, United Kingdom.

Submitted for consideration March 2017; accepted for publication in revised form September 2017.

Disclosure: The authors have no conflicts of interest to report.

This independent research is funded by the National Institute for Health Research [i4i, Turbocardia, II-LB-1111-20007]. Principal Investigator for the grant is Prof. T. Korakianitis. The views expressed in this publication are those of the authors and not necessarily those of the NHS, the National Institute for Health Research or the Department of Health. The PhD study of S. Mozafari is funded by a QMUL studentship.

Correspondence: Theodosios Korakianitis, ScD, Parks College of Engineering, Aviation and Technology, Saint Louis University, St. Louis, MO 63103. Email: korakianitis@alum.mit.edu.

DOI: 10.1097/MAT.0000000000000719

The design process of axial pumps is based on the similarity law of fluid dynamics. Two machines have equal efficiencies if they 1) are geometrically similar, 2) have similar velocity triangles at similar points in the flow path, 3) are performing in the same range of Reynolds number (Re), and 4) have working fluids with the same thermodynamic quality.[1] Cordier[2] collected experimental dimensionless characteristics of numerous pumps of different types and plotted them in an n_s–d_s graph based on their highest efficiency. The graphs show iso-efficiency curves of numerous industrial pumps based on their specific speed (n_s) and specific diameter (d_s), characteristic dimensionless numbers indicative of the rotational speed and rotor diameter, respectively. Each data point shows the highest efficiency of a pump corresponding to its dimensionless numbers. The Reynolds number, Re, is a characteristic dimensionless number that compares the inertia forces with the viscous forces in the fluid and indicates to what extent fluid flow is laminar or turbulent.

The equations and symbols for specific speed, specific diameter, and Reynolds number are presented in **Table 1**. In the above N_s is the rotor speed (rad/s), Q the volumetric flow rate (m^3/s), D the diameter (m), ρ the density of the working fluid (kg/m^3), Δp the pressure difference (N/m^2) from inlet to outlet of the pump, φ and ψ are flow and pressure coefficients, μ and ν are dynamic (Pa.s) and kinematic viscosity (m^2/s) of the fluid, respectively, C is the velocity (m/s) based on the cross-sectional area, and D is the hydraulic diameter (m).

The Cordier diagram was first presented in 1953 and following Balje's work in which industrial pumps were plotted on the diagram.[3] It has been used as a tool for the initial design phase in turbomachinery. Even with the advent of computational fluid dynamics (CFD) design, Cordier diagrams are embedded in common CFD software such as Ansys Vista CPD. Balje's diagram, however, corresponds to industrial pumps operating in the turbulent regime of Re = 10^8, whereas axial flow blood pumps operate in Re < 10^6.[4] Therefore, conditions 2 and 4 of the similarity law are not satisfied in this application and the conventional diagram is not suitable for blood pumps. Smith *et al*.[4,5] collected nondimensional data of 37 rotary blood pumps, including 7 axial, 2 mixed flow, and 28 radial pumps. The nondimensional characteristics were plotted on an n_s–d_s diagram to enable preliminary design of axial, centrifugal, and mixed flow pumps for ventricular assist devices (VADs) and mechanical circulatory support devices (MCSDs). Although the study was a pioneering work based on reliable experimental data, however, it mostly investigated centrifugal pumps and only a few data points of axial pumps were presented. Our recent paper[6] reported a nondimensional investigation, which

Table 1. Nondimensional Parameters

Parameter	Symbol	Equation
Specific speed	n_s	$n_s = \frac{N_s.\sqrt{Q}}{\left(\frac{\Delta p}{\rho}\right)^{0.75}} = \frac{\phi^{0.5}}{\psi^{0.75}}$
Specific diameter	d_s	$d_s = \frac{D.\left(\frac{\Delta p}{\rho}\right)^{0.25}}{\sqrt{Q}} = \frac{\psi^{0.25}}{\phi^{0.5}}$
Reynolds number	Re	$\frac{\rho CD}{\mu} = \frac{CD}{\nu}$

collected numerical data of 88 efficient centrifugal pumps and presented the data on a Cordier diagram. The graph is a specific tool to make a first estimation at the size, type, and performance of centrifugal blood pumps.

This article is a corresponding and similar contribution targeted at axial blood pumps. Sixty-two axial flow pump impellers are designed based on existing dimensionless experimental data,[4] numerical techniques, and conventional pump design methods.[1] The impellers were then manufactured, and a single-loop test rig (O-loop) was designed and developed to test the pump impellers in different operating conditions. The pump impellers were then modeled and studied with CFD to investigate the effect of design characteristics on the hemocompatibility of the device by modeling the induced hemolysis.

Prior study by Giersiepen *et al*.[7] on the hemolysis in a simple shear flow experiment showed that the hemolysis can be related to the shear stress and the exposure time through a power law equation. Based on the proposed power law equation, two types of computational models are used to computationally simulate the hemolysis.[7] The first is the Eulerian model in which the hemolysis index (HI) is integrated across the entire fluid domain at a single instant. The second approach is the Lagrangian model in which the HI is integrated along the red blood cell paths from the inlet to the outlet. The pros and cons of each method have been evaluated comprehensively in a study conducted by Taskin *et al*.[8] The study reported high percentage errors for both methods and that they could not accurately predict the hemolysis. However, the Eulerian approach showed high correlation coefficients, showing that it may be used for the comparison of different impellers by predicting the relative hemolysis. For this study, the highest efficiency of each pump was plotted in the previously produced n_s–d_s graph[6] to improve the diagram and enable preliminary design of centrifugal and axial pumps for MCSDs. The Normalised Index of Hemolysis (NIH) was simulated for each pump using the Eulerian approach. The effects of a change in rotor speed, blade number, and the blade angle on the hemolysis and efficiency were investigated.

Materials and Methods

In this article, axial rotors with varying outlet angle and number of blades are tested computationally and experimentally. Sixty-two rotor designs are tested computationally, yielding measures of hemolysis, and 62 corresponding rotors are then fabricated and tested experimentally in a blood analog (glycerol) solution yielding measures of efficiency. The experimental efficiencies are then plotted on the Cordier diagram.

Impeller Design

The required pressure rise and flow rate of the pump was defined from previous literature.[9,10] Some design parameters are assumptions made by the designer based on experience and previously designed pumps. Sixty-two axial pump impellers with varying outlet angle and number of blades are designed. The outlet angle (β_2) varied in the range 2–40° and the numbers of blades were 2, 4, and 6. The diameter was 22 mm. Due to interference at the hub, only five outlet angles could be fabricated for all numbers of blades: 20°, 25°, 30°, 35°, and 40°.

The blades were divided into three sections (hub, tip, and the mean effective diameter) and the velocity triangles were used to find the inlet angle and the twist on each section. The design procedure was developed as a MATLAB code that generates three-dimensional (3D) coordinates of the blade sections.[9–13] The profile and isometric view of a representative impeller with 2 blades and a 20° outlet angle is shown in **Figure 1**.

In general, the relatively high specific speed in the axial pumps dictates a smaller hub diameter, which leads to a greater flow area and thus greater flow rate and therefore a lower pressure rise. In this study, the hub-to-tip diameter ratio was determined based on our previous simulation results. To do so, the ratios of 0.15, 0.3, and 0.45 were simulated and the optimum ratio was selected. The simulations showed a relatively low pressure rise for the impeller with a 0.15 ratio because the blades were so thin. These impellers required higher rotational speeds in order to produce the design point pressure rise. The impeller with a 0.45 hub ratio had difficulty producing the required flow rate at low outlet angles due to the smaller flow area. Hence, the value of 0.3 was selected for the hub-to-tip ratio in this work.

Experimental Testing

Five impellers with high outlet angles (20°, 25°, 30°, 35°, and 40°) were manufactured with 2, 4, and 6 blades (15 in total) in order to study the effect of blade number on the performance of the pumps. The experimental O-loop includes several parts: a pump housing, a hand-operated Hoffman clip valve to change the resistance, an electromagnetic flow meter to measure the flow rate, two pressure transducers to measure the inlet and outlet pressures, a brushless DC motor (Maxon, EC max 22, 25 Watt), and a motor controller. The O-loop is shown in **Figure 2**.

The pressure upstream and downstream of the impeller and the corresponding flow rate were recorded at a 1 kHz sampling rate. The rotational speed was varied manually from 1,000 to 10,000 rpm in increments of 1,000 rpm. Rotational speeds of 4,000–7,000 were closest to the designed operating condition and consequently these results are selected for presentation here. At each speed the resistance of the system was changed by the Hoffman clip from fully open (no resistance) to fully closed (no flow). Measurements were taken at each quarter turn of the clip. The experiments were repeated three times in order to minimize uncertainty and verify the repeatability of the experiments.

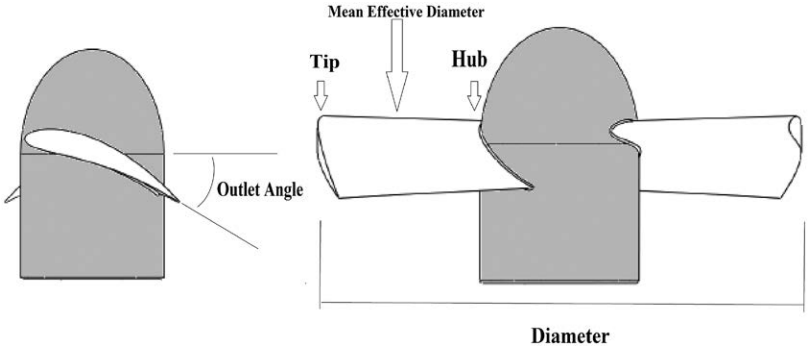

Figure 1. The profile and isometric view of a representative impeller with 2 blades and 20° outlet angle.

Computational Model

The 3D coordinates of the blades were generated and imported to ANSYS Fluid Flow (CFX). The incompressible Navier–Stokes equations were used to predict and calculate the flow fields in the pumps. The model has one rotating domain and it is defined by creating the fluid volume around the rotor surface. The rotational motion of the impeller is calculated using Multiple Reference Frame. In this approach, the flow is assumed steady state, the grid remains fixed, and the relative velocity is calculated throughout the domain.

Boundary conditions were specified to define the rotational speed, inlet pressure, and outlet flow rate. At the inlet, a relative pressure of 0 Pa was defined. At the outlet, a flow rate of 5 L/min was imposed. The solution was considered converged when the residual fell below 10^{-4}.

In this study, the k-epsilon turbulence model is used. The model uses the scalable wall-function approach[14] to improve robustness and accuracy when the near-wall mesh is very fine.

Although blood is a non-Newtonian fluid, for this part of the study blood was considered as an incompressible Newtonian fluid due to shear rates higher than 100/s in blood pumps. In this case, the non-Newtonian properties of blood such as shear thinning and viscoelasticity are negligible. A density of 1050 kg/m^3 and viscosity of 0.0036 Pa.s were defined for the working fluid.[15] A mesh independence study was performed, in a similar fashion to a study conducted by Fraser *et al*.,[16] to ensure a reliable result was obtained.

Shear Stress and Hemolysis Model

The shear stress induced on the fluid on each boundary is defined by:

$$\sigma = \left[\frac{1}{6}\Sigma\left(\sigma_{ii} - \sigma_{jj}\right)^2 + \Sigma(\sigma_{ij}\,\sigma_{ij})\right]^{1/2} \quad (1)$$

where i and j are perpendicular spatial dimensions. Shear-induced hemolysis was computed using the Eulerian-scalar-transport approach[8] in Equation 2:

$$\frac{d\left(\Delta\text{freeHB}'\right)}{dt} + v\rho.\nabla\left(\Delta\text{freeHB}'\right) = S \quad (2)$$

where ΔfreeHB′ is defined as a scalar variable equal to $\Delta\text{freeHB}^{\frac{1}{\alpha}}$ and ΔfreeHB is defined as plasma free hemoglobin, v is the mean inlet velocity (m/s), S is the source term defined as $S = \rho(\text{HB. C. }\sigma\beta)^{\frac{1}{\alpha}}$, in which HB is total blood

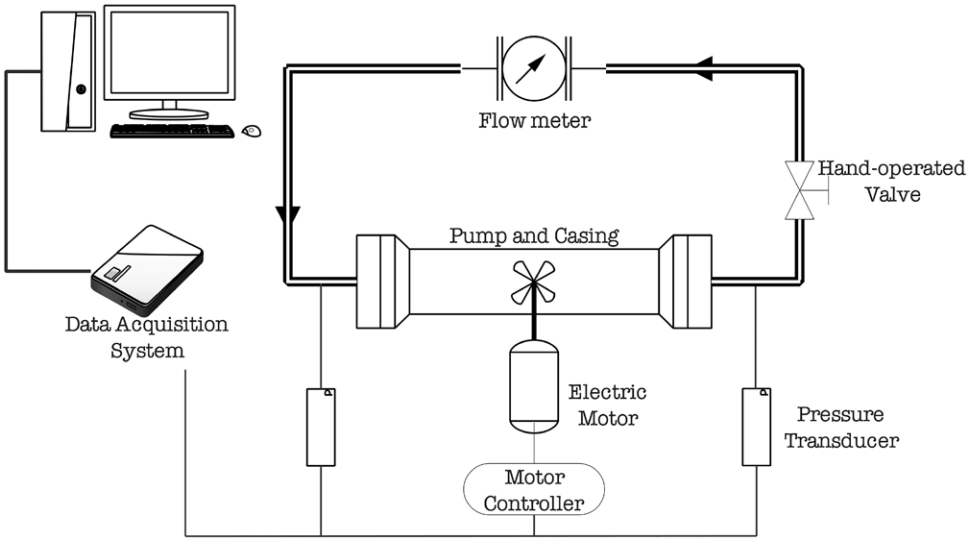

Figure 2. Schematic diagram of the O-loop test rig.

hemoglobin, ρ is the blood density, α = 0.785, β = 2.416, and $C = 3.62 \times 10^{-5}$ are constants.[7]

In order to express the degree of hemolysis, Normalized Index of Hemolysis (NIH) was calculated from Equation 3, adopted from the study by Arora *et al*.[17]:

$$\mathrm{NIH}(\mathrm{g}/100\mathrm{L}) = 100 \times \frac{\Delta \mathrm{freeHB}}{\mathrm{HB}} \times (1 - \mathrm{Hct}) \times k \qquad (3)$$

where Hct is the hematocrit and k is the hemoglobin content of blood and these quantities are 45% and ≈ 150 g/L, respectively, for a healthy person.[17] Based on the literature,[18] the critical value of 0.01 (g/100 L) has been established, where NIH higher than this value is defined as having an unacceptably high level of blood trauma.

Results

Q_{des} and H_{des} are the volumetric flow rate and pressure rise at the design point. Q/Q_{des} and H/H_{des} give the ratio of volumetric flow rate and pressure rise in a particular configuration compared with the design point. η is the experimentally measured hydraulic efficiency.

Figure 3 shows the values of estimated NIH in 14 two-bladed pumps with different outlet angles, rotating at 4,000–7,000 rpm. The critical NIH value has been marked with a dashed line. Higher outlet angle and higher rotational speed both result in greater hemolysis. **Figures 4** and **5** plot the efficiency and head ratio *versus* flow ratio for the same impellers at 6,000 rpm. The pressure rise is higher for higher outlet angles, as expected from previously reported experimental work.[1] **Figures 6** and **7** show the efficiency and head ratio of three impellers with the same characteristics with 2, 4, and 6 blades, also at 6,000 rpm. In this case fewer blades are more efficient. **Figure 8** shows the upgraded n_s–d_s diagram containing nondimensional data of more than 150 centrifugal[6] and axial pumps.

Discussion

The nondimensional approach of the study makes the results applicable to different performance characteristics and not just specific values. This will allow approximate sizing of blood pumps designed for the in-series configurations,[19–22] which may have different operating conditions from existing VADs.

The following discussion will describe in more detail the effect of number of blades, outlet angle, and rotational speed. The authors acknowledge the existence of other important factors that affect the performance of a blood pump such as blade-tip to housing clearance,[23] radial[24] and axial[25] clearances in flow paths, manufacturability,[26] inlet and outlet shapes,[27] and, particularly for axial pumps, flow straighteners to improve efficiency.[28] These parameters would be optimized after the initial sizing using the Cordier diagram created in this work and consequently are not examined in this more fundamental investigation. It is noted that flow straighteners, often included in axial MCSDs, will improve the efficiency of operation by reducing vortices in the flow downstream of the pump.

Number of Blades

Based on the theoretical and experimental equations for slip factor, the ideal flow guidance may be achieved by increasing the number of blades, so the flow leaves the impeller outlet at the outlet angle. However, beyond a particular value, the slip factor decreases due to increased blockage area. This value is considered a balance between the excessively high surface friction in pumps with too many blades and unguided diffusion in pumps with too few blades. The pressure rise results in **Figure 7** show this effect. At Q_{Des}, the 2 bladed impeller produced the lowest pressure rise among the three (≈0.9 H_{Des}). The 4 bladed impeller performed with the highest (≈1.2 H_{Des}) and the head ratio decreased to 1.1 H_{Des} for the impeller with 6 blades. It is apparent from **Figure 6** that efficiency is higher at a lower number of blades. However, this is the result of a constant rotational

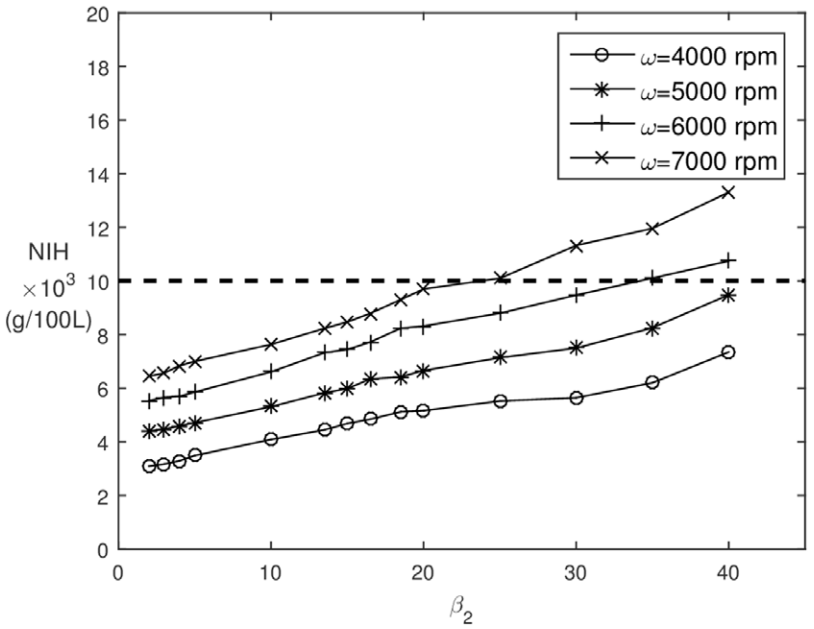

Figure 3. The simulated NIH for different outlet angles at four rotational speeds.

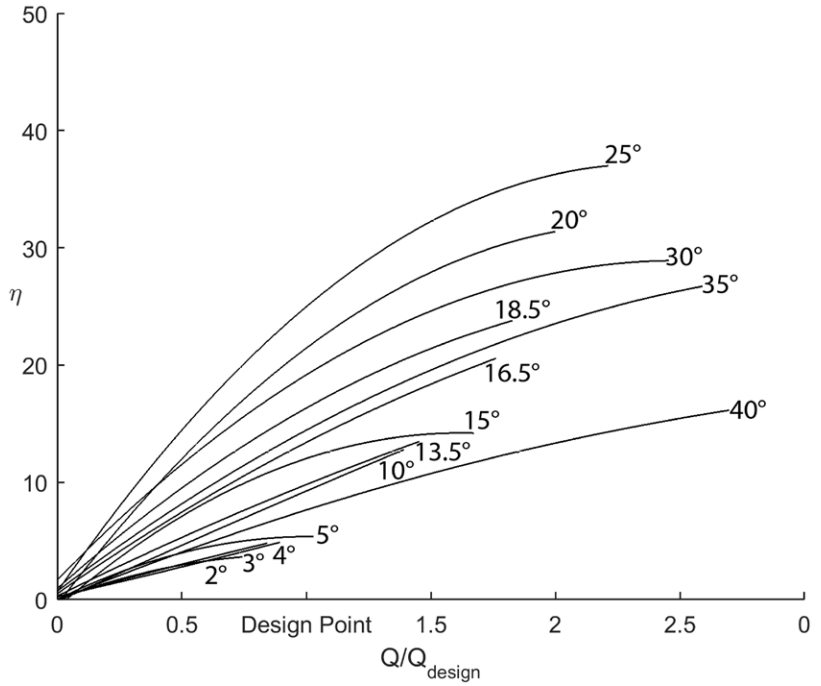

Figure 4. Efficiency *vs.* flow ratio for different outlet angles at 6,000 rpm.

speed, which leads to different values of pressure rise for the pumps, as shown in **Figure 7**. In order to compare the efficiencies meaningfully, the pumps must rotate at the various rotational speeds at which they produce the design point pressure rise. For this purpose, the rotational speeds were changed to 6,400, 5,300, and 5,500 rpm for the 2, 4, and 6 bladed impellers, respectively. The impellers produced the design point pressure rise at these speeds and achieved design point efficiencies of 18%, 19%, and 16%, respectively. This was implemented for the analysis of all five groups of impellers and overall showed very similar efficiencies for 2 and 4 bladed and slightly reduced efficiencies for 6 bladed impellers.

Outlet Angle

The effect of blade outlet angle on the pump performance was examining results from a group of 14 two-bladed impellers with a range of outlet angles. **Figures 4** and **5** compare the experimental efficiency and head ratio *versus* flow ratio for these impellers at 6,000 rpm. The results show that low

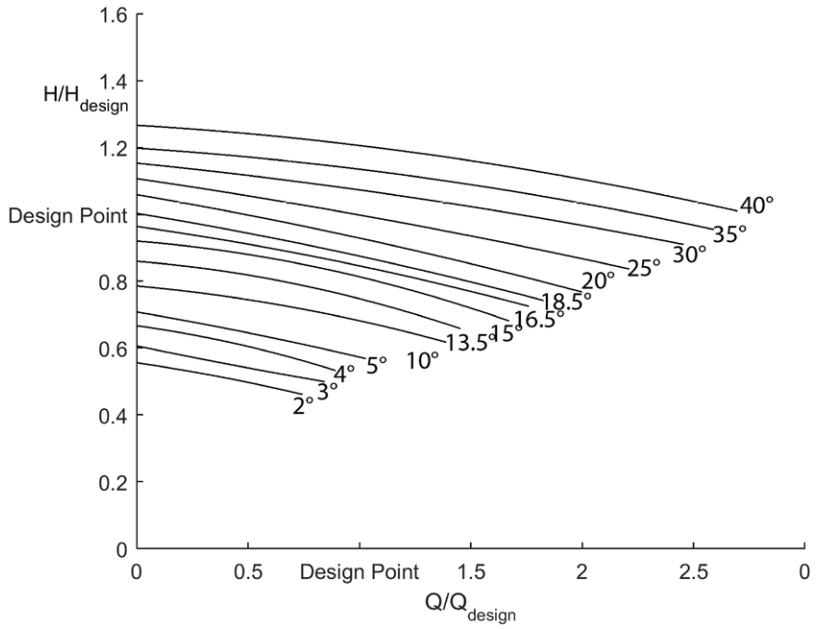

Figure 5. Head ratio *vs.* flow ratio for different outlet angles at 6,000 rpm.

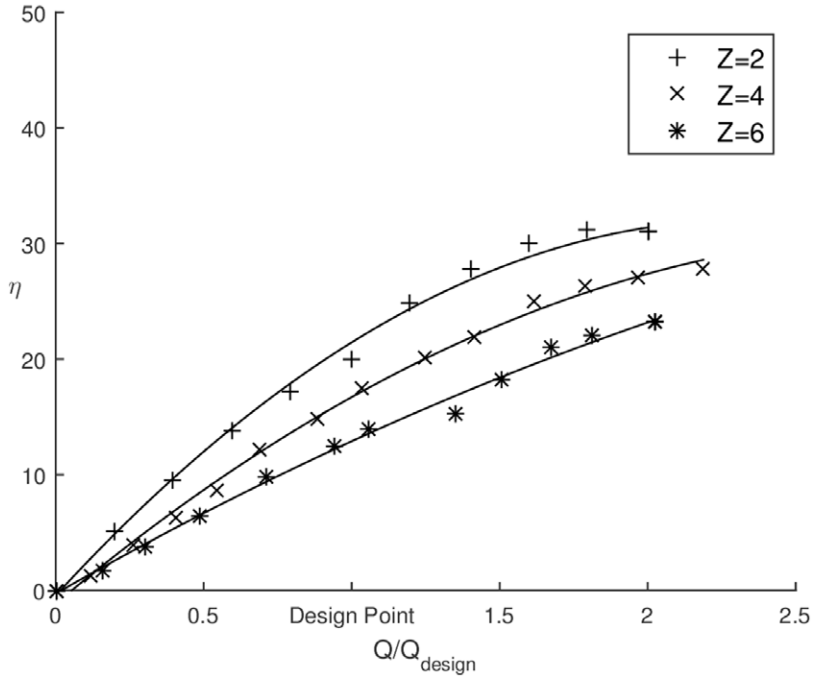

Figure 6. Efficiency *vs.* flow ratio for 2, 4, and 6 blades at 6,000 rpm.

outlet angles ($\beta_2 < 10°$) do not reach the required flow rate and slightly greater angles ($10° < \beta_2 < 15°$) may deliver the design point pressure rise, but fail to meet the required pressure rise at this rotational speed.

Increasing the rotational speeds for these pumps to reach the design point characteristics may lead to high shear stress and increase the probability of hemolysis. Impellers with higher outlet angles ($\beta_2 > 30°$) may reach both design point flow rate and pressure rise at relatively low speeds; however, the efficiency of the pump decreases at these outlet angles.

Hemolysis

In general this shows a higher value of NIH for higher rotational speeds and higher outlet angles. Although all outlet angles showed sufficiently low hemolysis at 4,000 and 5,000 rpm, angles higher than 35° and 20° cause excessive hemolysis at 6,000 and 7,000 rpm, respectively. At a constant speed, the lower blade angles are suitable for this application, due to the reduced probability of hemolysis. However, lower blade angles produce much lower pressure rise compared with higher angles. These impellers need higher rotational speeds

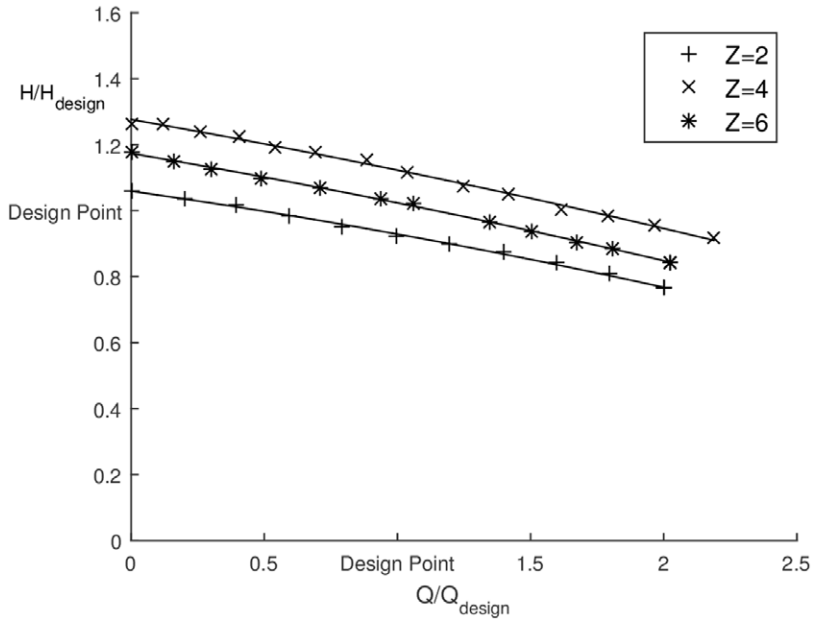

Figure 7. Head ratio *vs.* flow ratio for 2, 4, and 6 blades at 6,000 rpm.

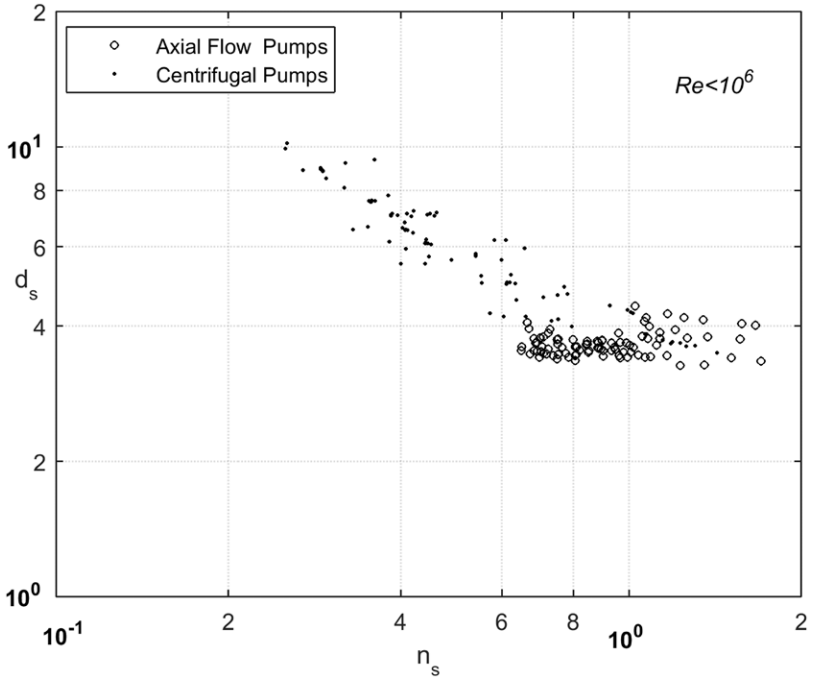

Figure 8. The upgraded n_s–d_s diagram containing nondimensional data of 150 centrifugal[6] and axial pumps.

in order to reach the design point flow rate and pressure rise. The higher rotational speed will increase the value of NIH and consequently there is a trade-off between the required pressure rise and NIH value in the pumps. An optimum angle should be determined to produce the required pressure head, while minimizing shear stress and thereby NIH.

Future Study

There is a significant interest in the field to modulate pump speeds, rather than operate at constant speed, to generate vascular pulsatility and phasic volume unloading. If the pump is pulsatile, it is working at a range of operating conditions throughout a single cycle. The diagrams in this work only show a single operating condition. This limitation could be overcome using a measure of the pump's efficiency in off-design condition, perhaps by an average efficiency across the rpm variation expected in the modulation scheme. It would be interesting in future to define these expected rpm ranges and examine whether the optimal pumps for design point operation are the same ones that perform best across this range.

Conclusions

Numerical, theoretical, and experimental techniques were used to characterize the performance of 62 pump impellers. The nondimensional characteristics of the tested axial pumps were collected and added to a previously produced graph for centrifugal pumps. Similar to Balje's existing work for industrial pumps, the axial flow pumps show a reduced dependence between n_s and d_s compared with their centrifugal counterparts. Hopefully, other pump designers will design more axial and centrifugal pumps and add their test results to the diagram. If blood pump developers analyze and add pump performance to this diagram, a more precise and reliable version of this diagram will be produced in future. Although there are many data points on this graph, it is still insufficient to predict a pattern for iso-efficiency lines. The completed chart would allow first estimation of the optimal axial impeller geometry for any desired operating condition. This tool allows greater efficacy in the initial phases of VAD design to reach optimal geometries, maximize efficiency, and minimize hemolysis.

References

1. Stepanoff AJ: *Centrifugal and Axial Flow Pumps*. New York, John Wiley & Sons, 1957.
2. Cordier, O: Similarity considerations in turbomachines. *VDI Report* 3(85): 955, 1955.
3. Balje O: *Turbomachines – A Guide to Design, Selection and Theory*. New York, John Wiley & Sons, 1981.
4. Smith WA, Allaire P, Antaki J, *et al*: Collected nondimensional performance of rotary dynamic blood pumps. *ASAIO J* 50: 25–32, 2004.
5. Smith WA, Allaire P, Antaki J, *et al*: Author reply to "Letter to the editor: A possible major mistake in the paper entitled "collected nondimensional performance of rotary dynamic blood pump"". *ASAIO J* 53(2): 255, 2004.
6. Korakianitis T, Rezaienia MA, Paul GM, Rahideh A, Rothman MT, Mozafari S: Optimization of centrifugal pump characteristic dimensions for mechanical circulatory support devices. *ASAIO J* 62: 545–551, 2016.
7. Giersiepen M, Wurzinger LJ, Opitz R, Reul H: Estimation of shear stress-related blood damage in heart valve prostheses–in vitro comparison of 25 aortic valves. *Int J Artif Organs* 13: 300–306, 1990.
8. Taskin ME, Fraser KH, Zhang T, Wu C, Griffith BP, Wu ZJ: Evaluation of Eulerian and Lagrangian models for hemolysis estimation. *ASAIO J* 58(4): 363–72, 2012.
9. Korakianitis T, Hamakhan IA, Rezaienia MA, Wheeler APS, Avital EJ Williams JJR: Design of high-efficiency turbomachinery blades for energy conversion devices with the three-dimensional prescribed surface curvature distribution blade design (CIRCLE) method. *Applied Energy* 89(1): 215–227, 2012.
10. Korakianitis T, Rezaienia MA, Hamakhan IA, Avital EJ, Williams JJR: Aerodynamic improvements of wind-turbine airfoil geometries

with the prescribed surface curvature distribution blade design (CIRCLE) method. *J Eng Gas Turbines Power* 134(8): 082601, 2012.
11. Massardo M, Satta A, Marini M: Axial-flow compressor design optimization. Part 2. Throughflow analysis. *J Turbomachin* 112(3): 405–410, 1990.
12. Korakianitis T, Rezaienia MA, Hamakhan IA, Wheeler APS: Two- and three- dimensional prescribed surface curvature distribution blade design (CIRCLE) method for the design of high efficiency turbines, compressors, and isolated airfoils. *J Turbomachin* 135(4): 041002, 1990.
13. Hamakhan IA, Korakianitis T: Aerodynamic performance effects of leading-edge geometry in gas-turbine blades. *Appl Energy* 87(5): 1591–1601, 2010.
14. Utyuzhnikov SV: Generalized wall functions and their application for simulation of turbulent flows. *Int J Numer Methods Fluids* 47(10–11): 1323–1328, 2005.
15. Pachidis V, Pilidis P, Talhouarn F, Kalfas A, Templalexis I: A fully integrated approach to component zooming using computational fluid dynamics. *J Eng Gas Turbines Power* 128(3): 579–584, 2006.
16. Fraser KH, Zhang T, Taskin ME, Griffith BP, Wu ZJ: A quantitative comparison of mechanical blood damage parameters in rotary ventricular assist devices: Shear stress, exposure time and hemolysis index. *J Biomech Eng* 134: 081002, 2012.
17. Arora D, Behr M, Pasquali M: Hemolysis estimation in a centrifugal blood pump using a tensor-based measure. *Artif Organs* 30: 539–547, 2006.
18. Nosé, Y. Design and development strategy for the rotary blood pump. *Artif Organs* 22(6): 438–446, 1998.
19. Shi Y, Korakianitis T: Numerical simulation of cardiovascular dynamics with left heart failure and in-series pulsatile ventricular assist device. *Artif Organs* 30: 929–948, 2006.
20. Ruiz P, Rezaienia MA, Rahideh A, Keeble TR, Rothman MT, Korakianitis T: *In vitro* cardiovascular system emulator (bioreactor) for the simulation of normal and diseased conditions with and without mechanical circulatory support. *Artif Organs* 37: 549–560, 2013.
21. Rezaienia MA, Paul G, Avital E, Rahideh A, Rothman MT, Korakianitis T: In-vitro investigation of cerebral-perfusion effects of a rotary blood pump installed in the descending aorta. *J Biomech* 49: 1865–1872, 2016.
22. Rezaienia MA, Paul G, Avital EJ, Mozafari S, Rothman M, Korakianitis T: In-vitro investigation of the hemodynamic responses of the cerebral, coronary and renal circulations with a rotary blood pump installed in the descending aorta. *Med Eng Phys* 40: 2–10, 2017.
23. Sinnott MD, Cleary PW. Effect of rotor blade angle and clearance on blood flow through a non-pulsatile, axial, heart pump. *Progr Comput Fluid Dynamics* 10(5–6): 300–306, 2010.
24. Paul G, Rezaienia A, Shen X, Avital E, Korakianitis T: Slip and turbulence phenomena in journal bearings with application to implantable rotary blood pumps. *Tribol Int* 104: 157–165, 2016.
25. Timms D, Fraser J, Hayne M, Dunning J, McNeil K, Pearcy M: The BiVACOR rotary biventricular assist device: Concept and *in vitro* investigation. *Artif Organs* 32: 816–819, 2008.
26. Paul G, Rezaienia A, Avital E, Korakianitis T: Machinability and optimization of shrouded centrifugal impellers for implantable blood pumps. *J Med Devices*, 11(2): 021005, 2017.
27. Inci G, Sorgüven E: Effect of LVAD outlet graft anastomosis angle on the aortic valve, wall, and flow. *ASAIO J* 58: 373–381, 2012.
28. Kawahito K, Benkowski R, Ohtsubo S, Noon GP, Nosé Y, DeBakey ME: Improved flow straighteners reduce thrombus in the NASA/DeBakey axial flow ventricular assist device. *Artif Organs* 21(4): 339–343, 1997.